Załącznik nr 46

Optical Gaussian beam interaction with one-dimensional thermal wave in the Raman–Nath configuration

Roman J. Bukowski

Institute of Physics, Silesian University of Technology, ul. Krzywoustego 2, 44-100 Gliwice, Poland
(rbukowski@polsl.pl)

Received 30 July 2008; revised 28 October 2008; accepted 31 October 2008;
posted 10 November 2008 (Doc. ID 99452); published 0 MONTH 0000

Optical Gaussian beam interaction with a one-dimensional temperature field in the form of a thermal wave in the Raman–Nath configuration is analyzed. For the description of the Gaussian beam propagation through the nonstationary temperature field the complex geometric optics method was used. The influence of the refractive coefficient modulation by thermal wave on the complex ray phase, path, and amplitude was taken into account. It was assumed that for detection of the modulated Gaussian beam parameters two types of detector can be used: quadrant photodiodes or centroidal photodiodes. The influence of such parameters as the size and position of the Gaussian beam waist, the laser–screen (detector) distance, the thermal wave beam position and width, as well as thermal wave frequency and the distance between the probing optical beam axis and source of thermal waves on the so-called normal signal was taken into account.

OCIS codes: 080.0080, 080.5692, 120.4290, 120.6810, 190.4870, 260.2710.

1. Introduction

The analysis of space–time distributions of temperature fields in various objects is useful for nondestructive testing of these objects' different characteristics. The usefulness of this research method stems from the combination of different ways of stimulating temperature fields and different ways of measuring and imaging these fields. Application of optical methods seems very favorable. Application of lasers makes it possible to generate temperature fields in various objects and samples easily by selecting the appropriate length of the light wave and also the power, the size of the laser beam, and ways of modulating the beam. The laser beam can also be used to detect the generated temperature field and for this purpose a tested object of various characteristics or its surrounding dependence on temperature is used.

One temperature field detection method is the refractive coefficient dependence on temperature, observed when rays of light are transmitted to the probe beam or its surrounding medium. This is the photodeflection method, which is also called the mirage effect. The theoretical description of this method was presented for the first time by Murphy and Aamodt [1,2]. They approximated the probing beam through a single light ray and used geometric optics methods to describe its propagation through the temperature field. In such a case only a probing ray deflection in the temperature field is taken into consideration. This theory was extended and is also included the case of a wide probing beam ("multiray") by using statistical methods [3–5].

It should be mentioned that taking limited sizes of the probing beam into account in photodeflectional investigations is important. Since the time-changed thermal field vanishes quickly because of its distance from the heat sources (see [6]), the large light beams used in those investigations are not reasonable, contrary to the acousto-optical Raman–Nath interaction where they are often applied. However in some acousto-optic applications focused optical Gaussian beams are also used (see [7]). Between the

0003-6935/09/0700C1-01$15.00/0

acousto-optic interaction and the photodeflection phenomenon there is a formal similarity: the acoustic wave in the former was replaced by a time–space-modulated thermal field in the latter. Because of this, similar methods can be used to describe both effects, but in the photodeflection phenomenon one should comply with the specific properties of the thermal fields.

The alternative for geometric optics is, naturally, wave optics. The wave description of the deflection method was presented by Glazov and Muratikov [8,9]. In order to describe a probing beam these authors used paraxial approximation and took into account its phase change caused by the temperature field. The advantage of the wave approach is the fact that it considers interaction of the whole probe beam and the temperature field at the same time. It should be noted that both theories include different aspects of the same phenomenon: deflection of the optical beam is caused by a refractive coefficient gradient in the transverse direction relative to the beam propagation direction, while allowing a change of phase in light waves generally describes changes in their propagation, including the wavefront form. Despite these differences, both theories correctly describe the results of measurements performed by means of the photodeflection method under the condition that suitable experimental setups fulfill the assumptions of the adequate theory.

It should be noticed that such a situation is quite strange. In every real photodeflection experiment the optical probing beam is influenced by deflection and changes of the phase as well. A correct theory describing such an experiment should include both effects. The phase effect within the confines of geometric optics (the complex one) was taken into account for the first time in the author's work [10] and was presented during the 7th Spring School on Acousto-Optics and Application organized by A. Sliwinski and his collaborators. The influence of both phase and deflection effects on the photodeflectional signal within the confines of complex geometric optics was presented for the first time in the work by Bukowski and Korte [11]. The problem was further developed at the Department of Applied Physics of the Institute of Physics of the Silesian University of Technology. The latest results were presented in [12–14].

In this work optical Gaussian beam interaction with temperature field in a one-dimensional thermal wave propagating in gas over the sample was analyzed. The configuration of interacting fields is analogous to the Raman–Nath acousto-optic interaction. To describe that interaction complex geometric optics methods were used, but a new form of analytical continuation to complex space of the refractive coefficient changes caused by a thermal wave was assumed. Thanks to that new form it was possible to abandon some approximations used in previous works, and the obtained results have wider application. Two kinds of a probing beam detector, a quadrant photodiode and a centroidal photodiode detector, were considered. The detector signal dependence on many parameters of the experimental setup was analyzed, especially the dependence on a probing beam radius and the location of its waist (or the location of an investigated sample). We also observed that the sample provided a screen that prevented a portion of the beam from reaching the detector.

2. Experimental Setup and Basic Equations

The scheme of the experimental setup that is analyzed in this work is shown in Fig. 1. The laser probing beam of a basic mode begins its run in the $z = 0$ plane, goes through the thermal wave field in gas over the sample, and falls into the detector. Depending on a beam height h over the sample and its radius b_s, in the sample region a part of the beam can be cut by the sample. It can be assumed that if $h > 2b_s$, cutting the beam by the sample is insignificant (the Gaussian beam transfers over 98% of its energy through a circular aperture of a radius of $2b_s$).

A. Geometric Optics Equations

Propagation of a harmonic light wave in an optically nonhomogeneous and isotropic medium can be approximately described by the scalar Helmholtz equation [15,16]:

$$\Delta u(\vec{r}) + k_0^2 \varepsilon(\vec{r}) u(\vec{r}) = 0, \tag{1}$$

where $u(\vec{r})$ is a spatial distribution of the wave electric field intensity (in the point $\vec{r}$), k_0 is its wavenumber in a vacuum, and $\varepsilon(\vec{r}) = n^2(\vec{r})$ describes the spatial distribution of the examined medium permittivity (square of the refraction coefficient). Within the confines of geometric optics, solutions of this equation are sought in the form [16]

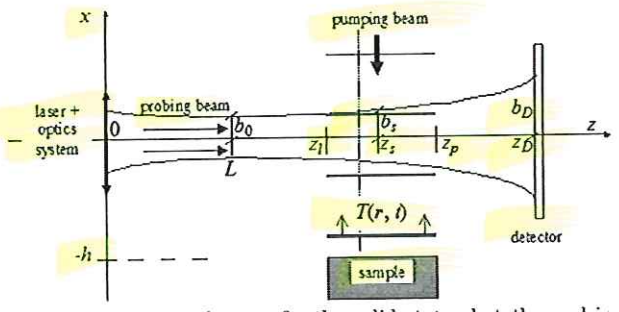

Fig. 1. Experimental setup for the solid state photothermal investigation with photodeflectional detection. The uniformly gas-heated region has a width of $\Delta z = z_p - z_l$, and its left edge is at a distance z_l from the system beginning (the light beam "input"). The light beam waist has a radius of b_0 and is placed at distance L from the beam "input." b_s and b_D are the probing beam radii over the sample center and at the detector, respectively. The probing beam axis runs at height h over the sample surface and is perpendicular to the thermal wave column (Raman–Nath configuration). The detector plane coordinate is equal to z_D.

$$u(\vec{r}) = A(\vec{r})\exp(ik_0\psi(\vec{r})), \qquad A(\vec{r}) = \sum_{m=0}^{\infty} \frac{A_m(\vec{r})}{(ik_0)^m}. \quad (2)$$

Here, the quantity $\psi(\vec{r})$ is called wave eikonal, and the wave amplitude $A(\vec{r})$ expansion in the series relative to wavenumber reverse powers is called the Debye expansion or the Luneburg–Klein expansion. Equations for the eikonal and amplitudes of m orders (transport equations) have the form

$$\begin{cases} (\vec{\nabla}\psi)^2 = n^2(\vec{r}) \\ 2(\vec{\nabla}A_0)\circ(\vec{\nabla}\psi) + A_0\Delta\psi = 0 \\ 2(\vec{\nabla}A_m)\circ(\vec{\nabla}\psi) + A_m\Delta\psi = -\Delta A_{m-1}, \qquad m = 1,2,\ldots \end{cases} \quad (3)$$

In geometric optics formalism, the solutions for these equations are sought using the Hamilton method, which leads to the following equations for light rays:

$$\begin{cases} \frac{d\vec{r}}{d\tau} = \vec{p} \\ \frac{d\vec{p}}{d\tau} = \frac{1}{2}\vec{\nabla}n^2(\vec{r}) \end{cases}, \qquad \begin{cases} \vec{p} = \vec{\nabla}\psi \\ \frac{d\psi}{d\tau} = \vec{p}^2 = n^2(\vec{r}) \end{cases}. \quad (4)$$

Here, $\vec{p}$ means a ray momentum and τ is a running coordinate along the ray. The ray goes out from the point of the coordinates (ξ,η) defined on the given output surface (in this case the plane $z = 0$). On this surface the amplitudes distribution A_m and the eikonal ψ must be given (boundary conditions). General solutions for the eikonal equation and the zero order amplitude equation are as follows:

$$\psi(\tau) = \psi^0(\xi,\eta) + \int_0^{\tau} n^2[\vec{r}(\tau')]\mathrm{d}\tau',$$
$$A_0(\tau) = A_0(0)\left[\frac{D(0)}{D(\tau)}\right]^{1/2}, \quad (5)$$

where $D(\tau)$ is a Jacobian determinant of a transition from ray coordinates (ξ,η,τ) to Cartesian coordinates (x,y,z). Integration in relation for the eikonal is done along the ray's trajectory. It was assumed that on the output plane $z = 0$ we have $\tau = 0$.

B. Gaussian Beam in a Homogeneous Medium

If the boundary conditions are assumed in the form of the Gaussian amplitude distribution of the electric field intensity in the output plane, the application of the above equations to an optically homogeneous medium with refractive coefficient n_0 leads to the propagation into the OZ axis positive direction beam's relation for the basic Gaussian mode [10,17,18]

$$u(\xi,\eta,\tau) \cong E_0\frac{z_{Rc}}{z_{Rc}+in_0\tau}\exp\left[ik_0n_0\left((n_0\tau - L) + i\frac{\xi^2+\eta^2}{2z_R}\frac{z_{Rc}}{z_R}\right)\right], \quad (6)$$

but the rays' equations are as follows:

$$\begin{cases} x = \xi\left(1 + i\frac{n_0\tau}{z_{Rc}}\right) \\ y = \eta\left(1 + i\frac{n_0\tau}{z_{Rc}}\right) \\ z = n_0\tau\sqrt{1 + \frac{\xi^2+\eta^2}{z_{Rc}^2}} \end{cases}. \quad (7)$$

Here we have $z_{Rc} = z_R - iL$ and $z_R = k_0n_0{b_0}^2$, where b_0 is the intensity radius of the Gaussian beam in its waist. The quantity z_R is called a Rayleigh length for the given Gaussian beam, and z_{Rc} can be called a complex Rayleigh length for that beam. E_0 is the electric field intensity on the beam's axis in the output plane. It can be seen that the rays run in the complex space. Determination of the electric field intensity distribution of that beam in the detection place demands solutions for Eq. (7) relative to ray coordinates ξ, η and τ. It is a nonlinear setup, and it is usually solved by linearization with application of the paraxial approximation $|(\xi^2+\eta^2)/z_{Rc}^2| \ll 1$.

C. Thermal Waves in Gas Over the Sample

The form of the temperature distribution in gas over the sample depends on many details of the experimental setup, which manifest themselves in adequate equations and boundary conditions. In this work a model situation was considered. The assumptions were as follows: 1°, the temperature distribution in gas over the sample is described by the Fourier–Kirchhoff equation for a homogeneous medium; 2°, a stimulated beam provides an energy stream that is even on the whole surface of the sample and stationary harmonically in time with an angular frequency Ω; 3°, changes of gas temperature in areas that are not located directly over the sample can be omitted; 4°, continuity conditions for temperature and heat flux are valid on the border of the sample and gas; 5°, the sample sizes in transverse direction relative to the probing beam are much bigger than the beam diameter over the sample. In such a situation the temperature distribution in the region over the sample is a one-dimentional distribution and shows a so-called thermal wave:

$$T(x,z) - T_0 = \vartheta(x,z) = [\theta_g + \vartheta_g\exp(-k_g(x+h)) \times \cos(\Omega t - k_g(x+h) + \gamma_g)]\Delta H(z;z_l,z_p). \quad (8)$$

In this formula the following symbols were used: $k_g = [\Omega/(2\kappa_g)]^{1/2}$ = wavenumber of the thermal wave, T_0 is the surrounding temperature (constant), κ_g is the thermal diffusivity of the gas, γ_g is the phase shift between the stimulated beam and the sample

surface temperature, θ_g is the constant gas temperature increase over the sample, and ϑ_g is the harmonic amplitude of temperature changes on the sample surface. Furthermore, $\Delta H(z; z_l, z_p) = H(z - z_p) - H(z - z_l)$, where $H(\zeta)$ represents the Heaviside step function. It can be seen that, although the Fourier–Kirchhoff equation is not a wave equation, its solution has a wave character because harmonic boundary conditions were applied. The characteristic of these thermal waves is that their wavenumber and attenuation coefficient depend on the wave frequency and always have the same quantity. This means that these waves are strongly damped waves with a strong dispersion. Their group velocity in the air for frequency $f = 100\,\mathrm{Hz}$ amounts to about $0.33\,\mathrm{m/s}$. Furthermore, it should be mentioned that the parameters ϑ_g, θ_g, and γ_g depend significantly on the sample characteristics and that the aim of photodeflectional measurements is to gain these parameters' quantities.

3. Probing Gaussian Beam Interaction with a Thermal Wave

A thermal wave in gas causes space–time changes of the refractive coefficient of the gas. A probing light beam propagating in such an optically nonhomogeneous medium changes its parameters. Whithin the confines of geometric optics the following effects in thermal wave's influence on the probing light beam's propagation can be distinguished:

1° Phase effect, the refractive coefficient change causes the change of the probing beam phase (of the light ray) and thus the change of its eikonal; these changes depend on refractive coefficient changes along the probing beam propagation direction.

2° Deflection effect, a refractive coefficient change causes a beam (ray) propagation direction (continuous) change; these changes depend on refractive coefficient gradient in the perpendicular direction relative to probing beam propagation direction.

3° Refractive effect, a refractive coefficient step change on the borders of the area with the thermal wave causes probing beam (rays) refraction, i.e., propagation direction step changes.

4° Amplitude effect, refractive coefficient changes cause a beam divergence change and thus a wave (ray) amplitude space distribution change.

It should be emphasized that usually these effects do not appear in a pure form but are reciprocally conjugated. For example, beam deflection generally entails beam phase changes, and its divergence changes as well, and thus amplitude changes. Within the confines of geometric optics such "conjugate effects" are also considered.

A. Dielectric Permittivity in Gas with a Thermal Wave

In standard photodeflection measurements global temperature changes of the sample and surrounding gas are at the level 1 K and the temperature changing amplitudes are at the level of millikelvins. In this situation it is possible to limit to a linear factor describing temperature's influence on the refractive coefficient change:

$$n(T) = n_0 + \left.\frac{dn}{dT}\right|_{T_0} (T - T_0) = n_0 + n_0 s_T (T - T_0), \tag{9}$$

where s_T is the temperature sensitivity of the refractive coefficient. In that case a gas electric permittivity in a thermal wave region is expressed by the relationship

$$\varepsilon(T) = n^2(T) = n_0^2 + \nu(\vec{r}), \qquad \nu(\vec{r}) \cong 2n_0^2 s_T \vartheta(x, z). \tag{10}$$

Here $\nu(\vec{r})$ means medium electric permittivity disturbances caused by a thermal wave. Equation (10) should be used in Eq. (1) and in the equations that follow. However, refractive coefficient thermal sensitivities for gases are of the order of $-5 \times 10^{-6}\,\mathrm{K}^{-1}$, which in combination with a gas temperature causes changes in the amplitude in thermal waves of the order of $10^{-3}\,\mathrm{K}$ means that the refractive coefficient changes amplitude is of the order of 10^{-8}. In this situation it is justified to apply a perturbation calculus in calculations, but the product $s_T \cdot \vartheta_g$ plays the role of a perturbation parameter.

As has already been mentioned, in a geometric description a Gaussian beam consists of rays that run in a complex space. In that case the problem of the analytic continuation of Eq. (10) to the complex space is of great importance. In former works (for example, [10,12]) Eq. (10) was directly used, and in them x and y coordinates took complex values. Taking into consideration the fact that in the end only the real part of obtained solutions has physical sense, it is possible to complete Eq. (10) with an adequately matched imaginary part. A considerable simplification of the calculations may be expected when in Eq. (10) the cosine's trigonometric function is replaced with an exponential function of an adequate imaginary argument:

$$\nu(\vec{r}) \cong 2n_0^2 s_T \vartheta_c(x, z), \tag{11}$$

$$\vartheta_c(x, z) = [\theta_g + \vartheta_g \exp(\varphi_t) \exp(-k_{gc} x)] \Delta H(z; z_l, z_p), \tag{12}$$

where

$$k_{gc} = (1 + i) k_g, \qquad \varphi_t = i(\Omega t + \gamma_g) - k_{gc} h. \tag{13}$$

In many cases the signal from the photodetector is measured by means of a lock-in amplifier. Then in

Eq. (12) the constant component θ_g can be omitted. Such a situation will be examined below.

B. Corrections to Ray Trajectories, to the Eikonal, and to Ray Amplitudes in a Probing Beam

Corrections to rays trajectories in the first order of perturbation calculus are determined by the relation [16]

$$\vec{r}_1 = \int_0^{\tau} (\tau - \tau') \frac{1}{2} \vec{\nabla} \nu(\vec{r}_0(\tau')) \mathrm{d}\tau'. \tag{14}$$

Here $\vec{r}_0(\tau')$ is the ray trajectories in a nondisturbed beam equation [Eqs. (7)]. Because of this the corrections are as follows:

$$x_1 = s_T \vartheta_g \frac{z_{Rc}}{k_{gc}\xi^2} \exp(\varphi_t) \times \left\{ \left[1 - k_{gc}\xi \frac{in_0(\tau - \tau_p)}{z_{Rc}} \right] \exp\left[-k_{gc}\xi \left(1 + \frac{in_0\tau_p}{z_{Rc}} \right) \right] - \left[1 - k_{gc}\xi \frac{in_0(\tau - \tau_l)}{z_{Rc}} \right] \exp\left[-k_{gc}\xi \left(1 + \frac{in_0\tau_l}{z_{Rc}} \right) \right] \right\}. \tag{15a}$$

$$y_1 = 0, \tag{15b}$$

$$z_1 = s_T \vartheta_g \frac{n_0 \exp(\varphi_t)}{\sqrt{1 + (\xi^2 + \eta^2)/z_{Rc}^2}} \left\{ (\tau - \tau_l) \exp\left[-k_{gc}\xi \left(1 + \frac{in_0\tau_l}{z_{Rc}} \right) \right] - (\tau - \tau_p) \exp\left[-k_{gc}\xi \left(1 + \frac{in_0\tau_p}{z_{Rc}} \right) \right] \right\}. \tag{15c}$$

In Eqs. (15) the following designations were used: $\tau_l = \tau(z_l)$ and $\tau_p = \tau(z_p)$. These formulas are true in the region $\tau \geq \tau_p$, that is, behind the sample.

The correction to the eikonal in the applied perturbation calculus is described by the formula [16]

$$\psi^1(\xi, \eta, \tau) = \frac{1}{2} \int_0^{\tau} \nu(\vec{r}(\tau')) \mathrm{d}\tau'. \tag{16}$$

The integration here should take place along the corrected ray trajectory. However, the corrections (15) to the ray trajectory are proportional to the perturbation parameter $s_T \cdot \vartheta_g$, like the medium electric permittivity disturbance ν. In that case taking into consideration in Eq. (16) corrections to the ray trajectory would also mean taking into consideration in calculations corrections of at least second order relative to the disturbance parameter, which on that level of accuracy is not justified. In that case, if in Eq. (16) we take into consideration the dependence [Eq. (7)] in the region $\tau \geq \tau_p$ we obtain

$$\psi^1(\xi, \eta, \tau) = s_T \vartheta_g \frac{in_0 z_{Rc}}{k_{gc}\xi} \exp(\varphi_t) \left\{ \exp\left[-k_{gc}\xi \left(1 + \frac{in_0\tau_p}{z_{Rc}} \right) \right] - \exp\left[-k_{gc}\xi \left(1 + \frac{in_0\tau_l}{z_{Rc}} \right) \right] \right\}. \tag{17}$$

The ray amplitude is described by the second formula given in Eq. (5). Within the confines of the first order accuracy relative to the disturbance parameter and without paraxial corrections, which for the Gaussian beam are considered only in its eikonal, we can write the Jacobian of the transition from ray to Cartesian coordinates in the form

$$D(\tau) \cong \frac{\partial x_0}{\partial \xi} \frac{\partial y_0}{\partial \eta} \frac{\partial z_0}{\partial \tau} + \frac{\partial x_1}{\partial \xi} \frac{\partial y_0}{\partial \eta} \frac{\partial z_0}{\partial \tau} + \frac{\partial x_0}{\partial \xi} \frac{\partial y_0}{\partial \eta} \frac{\partial z_1}{\partial \tau} = D^0(\tau) + D^1(\tau), \tag{18}$$

where x_0, y_0, and z_0 are described in Eqs. (7), and x_1 and z_1 in Eqs. (15). This gives us

$$A(\tau) \cong A^0(\tau)[1 + a^1(\tau)]. \qquad a^1(\tau) = -\frac{1}{2} \left[\frac{\partial x_1/\partial \xi}{\partial x_0/\partial \xi} + \frac{\partial z_1/\partial \tau}{\partial z_0/\partial \tau} \right], \tag{19}$$

where $A^0(\tau) = E_0 z_{Rc}/(z_{Rc} + in_0\tau)$ results from Eq. (6) and

$$a^1(\tau) = \frac{1}{2} s_T \vartheta_g \exp(\varphi_t) \left\{ a_p^1(\tau) \exp\left[-k_{gc}\xi \left(1 + \frac{in_0\tau_p}{z_{Rc}} \right) \right] - a_l^1(\tau) \exp\left[-k_{gc}\xi \left(1 + \frac{in_0\tau_l}{z_{Rc}} \right) \right] \right\}, \tag{20}$$

$$a_r^1(\tau) = 1 - \frac{z_{Rc}^2}{k_{gc}\xi \left(1 + \frac{in_0\tau}{z_{Rc}} \right)} \left[k_{gc}^2 \left(1 + \frac{in_0\tau_r}{z_{Rc}} \right) \frac{in_0(\tau - \tau_r)}{z_{Rc}} - \frac{1}{\xi} \left(k_{gc} \left(1 - \frac{in_0(\tau - 2\tau_r)}{z_{Rc}} \right) + \frac{2}{\xi} \right) \right], r = l, p. \tag{21}$$

C. Inverse Problem of Geometric Optics

The obtained expressions enable us to describe the electric field intensity distribution in a probing beam after interaction with a thermal wave but relative to the ray coordinates:

$$u(\xi, \eta, \tau) = A^0(\tau)[1 + a^1(\tau)] \times \exp\{ik_0[\psi^0(\xi, \eta, \tau) + \psi^1(\xi, \eta, \tau)]\}, \tag{22}$$

where on the basis of Eq. (6) we have

$$\psi^0(\xi,\eta,\tau) = n_0\left[(n_0\tau - L) + i\frac{\xi^2+\eta^2}{2z_R}\frac{z_{Rc}}{z_R}\right]. \quad (23)$$

In order to determine the light intensity distribution in the place of detection $\vec{r}_D = (x_D, y_D, z_D)$ we need to solve the so-called geometric optics inverse problem, that is, to express the ray coordinates by the detection point Cartesian coordinates. In that case the following system of equations should be solved:

$$\begin{cases} x_D = x_0(\xi_D,\eta_D,\tau_D) + x_1(\xi_D,\eta_D,\tau_D) \\ y_D = y_0(\xi_D,\eta_D,\tau_D) \\ z_D = z_0(\xi_D,\eta_D,\tau_D) + z_1(\xi_D,\eta_D,\tau_D) \end{cases}, \quad (24)$$

where nondisturbed coordinates are described by Eqs. (7) and corrections to ray trajectories are described in Eqs. (15). That is, a system of nonlinear equations and its solutions should be looked for after the linearization with the first order accuracy relative to perturbation parameter and paraxial corrections. In that case it should be assumed that

$$\begin{aligned} x_1(\xi_D,\eta_D,\tau_D) &\cong x_1(\xi_{D0},\eta_{D0},\tau_{D0}) = x_{10}, \\ z_1(\xi_D,\eta_D,\tau_D) &\cong z_1(\xi_{D0},\eta_{D0},\tau_{D0}) = z_{10}, \end{aligned} \quad (25)$$

and that

$$\xi_D = \xi_{D0} + \xi_{D1}, \quad \eta_D = \eta_{D0} + \eta_{D1}, \quad \tau_D = \tau_{D0} + \tau_{D1}, \quad (26)$$

where ξ_{D0}, η_{D0}, and τ_{D0} are the solutions of Eqs. (7) in the detection point. In addition, $|\xi_{D1}| \ll |\xi_{D0}|$, $|\eta_{D1}| \ll |\eta_{D0}|$, and $|\tau_{D1}| \ll |\tau_{D0}|$ must also be valid. In that case the solution of the system of equations takes the form of

$$\begin{cases} \tau_{D1} \cong \frac{x_D z_D}{n_0 z_{RD}^2} x_{10} - \frac{1}{n_0}\left(1 + i\frac{x_D^2+y_D^2}{z_{RD}^2}\frac{z_D}{z_{RD}}\right) z_{10} \\ \eta_{D1} \cong -i\frac{x_D y_D z_D z_{Rc}}{z_{RD}^4} x_{10} + i\frac{y_D z_{Rc}}{z_{RD}^2} z_{10} \\ \xi_{D1} \cong -\frac{z_{Rc}}{z_{RD}}\left(1 - i\frac{x_D^2}{z_{RD}^2}\frac{z_D}{z_{RD}}\right) x_{10} + i\frac{x_D z_{Rc}}{z_{RD}^2} z_{10} \end{cases}, \quad (27)$$

where $z_{RD} = z_{Rc} + iz_D$. As has already been mentioned, paraxial corrections in these expressions should be taken into account while calculating the eikonal, but they can be omitted when calculating the ray amplitude.

D. Probing Beam Light Intensity Distribution on the Detector Plane

After Eqs. (26) and (27) have been substituted to the formula of the probing beam eikonal after its interaction with the thermal wave it turns out that all corrections compensate for one another, and in the end we get the nondisturbed beam's eikonal:

$$\begin{aligned} \psi(\xi_D,\eta_D,\tau_D) &\cong \psi^0(\xi_D,\eta_D,\tau_D) + \psi^1(\xi_{D0},\eta_{D0},\tau_{D0}) \\ &= \psi_{D0}(\vec{r}_D) = n_0(z_D - L) + in_0\frac{x_D^2+y_D^2}{2z_{RD}}. \end{aligned} \quad (28)$$

This is a specific situation in the perturbation calculus for geometric optics. It results from special characteristics of thermal waves, and especially from the fact that the damping coefficient of these waves equals their wavenumber. Corresponding changes in the investigated beam eikonal may appear in the second order of perturbation calculus. It results from Eq. (28) that the Gaussian probing beam, after passing a thermal wave field in the investigated configuration, still is a Gaussian beam. However, its amplitude distribution differs from a corresponding distribution of a nondisturbed beam. By substituting Eqs. (26) and (27) into Eqs. (19) and (20) we get

$$A(\vec{r}_D) \cong E_0\frac{z_{Rc}}{z_{RD}}[1 + a_{D1}(\vec{r}_D)]. \quad (29)$$

$$\begin{aligned} a_{D1}(\vec{r}_D) = s_T\vartheta_g &\frac{1}{2k_{gc}x_D^3 z_{RD}^2}\exp(\varphi_t) \\ &\left[a_l^1(\vec{r}_D)\exp\left(-k_{gc}x_D\frac{z_{Rp}}{z_{RD}}\right)\right. \\ &\left. - a_p^1(\vec{r}_D)\exp\left(-k_{gc}x_D\frac{z_{Rl}}{z_{RD}}\right)\right], \end{aligned} \quad (30)$$

where

$$\begin{aligned} a_r^1(\vec{r}_D) = {} & k_{gc}[z_{RD}^2 - 2z_{Rc}(z_{RD} - z_{Rr})]x_D^3 \\ & + z_{RD}[k_{gc}^2 z_{RD} z_{Rr}(z_{RD} - z_{Rr}) - 2(z_{RD} - z_{Rc})]x_D^2 \\ & + k_{gc}z_{RD}^3(z_{RD} - 2z_{Rr})x_D - 2z_{RD}^4, r = l, p. \end{aligned} \quad (31)$$

In addition $z_{Rr} = z_{Rc} + iz_r$, $r = l, p$.

Light intensity I in the probing beam on the detector is proportional to $|u|^2$. When we take into consideration that $|a_{D1}| \ll 1$, we get

$$\begin{aligned} I(\vec{r}_D) &\cong I_{G0}(\vec{r}_D) + 2\mathrm{Re}(a_{D1}(\vec{r}_D))I_{G0}(\vec{r}_D) \\ &= I_{G0}(\vec{r}_D) + I_V(\vec{r}_D). \end{aligned} \quad (32)$$

where I_{G0} means the light intensity distribution in the nondisturbed beam. Here an important meaning has the component I_V, which includes information about a thermal wave influence on the probing beam. This component is proportional to $|\exp(\varphi_t)|$, which means that the light intensity is modulated with the frequency of the temperature field in thermal

wave modulation. Thanks to this, this component can be easily measured using the lock-in amplifier.

4. Photodeflection Signal

After passing the region of an interaction with a thermal wave, the probing beam falls on the photodetector located perpendicular to the probing nondisturbed beam axis. Usually, a quadrant photodiode or a centroid photodiode is used as a detector. The photodiode changes the light signal into an electric signal. Generally probing rays undergo deflection in planes XZ and YZ as well, which are normal and parallel to the sample surface, respectively. In the first case the detector measure is the so-called normal photodeflection signal, and in the second case it is the tangential (or transverse) one. In the considered case only the probing beam deflection in the XZ plane is possible [see the correction to the ray trajectories in Eqs. (15)], so that only the normal phododeflection signal can be detected.

A. Quadrant Photodiode

The current signal from the quadrant diode can be written as

$$F^{(q)} = \sum_i F_i^{(q)} = \sum_i \sigma_i K_q \int_{S_{Di}} I_V(\vec{r}_D)\mathrm{d}S_D, \tag{33}$$

where integration takes place on adequate active (illuminated) parts of the photodiode surface (in the case of quadrant photodiode on the illuminated parts of its quadrants or halves) and the obtained currents are added or subtracted electronically ($\sigma_i = \pm 1$). K_q means the detector's sensitivity. In that case the normal photodeflection signal, on the basis of Eq. (33), can be written as

$$\begin{aligned} F_n^{(q)} &= K_q \int_{-\infty}^{+\infty} \mathrm{d}y_D \left(\int_0^{+\infty} - \int_{-h_D}^{0} \right) \mathrm{d}x_D I_V(\vec{r}_D) \\ &= 2K_q \mathrm{Re}\left[\int_{-h_D}^{+\infty} \mathrm{sgn}(x_D) a_{D1}(x_D, z_D) I_{G0x}(x_D)\mathrm{d}x_D \right]. \end{aligned} \tag{34}$$

where it was taken into account that the sample partially screens one of the detector's halves [in the region $(-\infty, -h_D)$, $\mathrm{sgn}(x_D) = -1$ for $x_D < 0$ and $\mathrm{sgn}(x_D) = 1$ for $x_D > 0$]. Other limits of the integration were moved to $\pm\infty$ because of the fast disappearance of the light intensity in the Gaussian beam along with the distance from its axis. In addition it was assumed that the center of the detector is on the axis of the nondisturbed probing beam. Integrating on y_D is elementary because a_{D1} does not depend on y_D:

$$\begin{aligned} I_{G0x}(x_D) &= \int_{-\infty}^{+\infty} I_{G0}(\vec{r}_D)\mathrm{d}y_D \\ &= I_{0D} \int_{-\infty}^{+\infty} \exp\left[\frac{-(x_D^2 + y_D^2)}{b_D^2}\right] \mathrm{d}y_D \\ &= \frac{P_G}{\sqrt{\pi} b_D} \exp\left(\frac{-x_D^2}{b_D^2}\right). \end{aligned} \tag{35}$$

Here b_D is the intensity radius of the nondisturbed probing beam on the detector, $b_D = b_0[1 + (z_D - L)/{z_R}^2]^{1/2}$, where b_0 is the intensity radius of the probing beam in its waist. Besides, I_{0D} is the light intensity on the axis of the nondisturbed probing beam, which falls on the detector, and P_G is this beam's power.

B. Centroid Photodiode

Thanks to the adequate construction the normal photodeflectional signal from the centroidal photodiode for the assumed interaction geometry is described by the formula (see [19])

$$\begin{aligned} F_n^{(c)} &= K_c \int_S x_D I_V(\vec{r}_D)\mathrm{d}S_D \\ &= 2K_c \mathrm{Re}\left[\int_{-h_D}^{+\infty} x_D a_{D1}(x_D, z_D) I_{G0x}(x_D)\mathrm{d}x_D \right]. \end{aligned} \tag{36}$$

where it was taken into consideration once again that in the investigated configuration a_{D1} does not depend on y_D. In some works the function $I_{G0}(x_D, y_D = 0)$ is used instead of function $I_{G0x}(x_D)$, which is equivalent to the formula above but with another detector's sensitivity K_c.

C. Final Signal

The integration in Eq. (36) was fulfilled exactly (analytically) in one case: the lack of detector screening ($h_D \to \infty$). In other cases, while calculating integrals (34) and (36) approximate methods were used. Expansion of the adequate expressions into series ensured sufficient accuracy. After having done the already mentioned integrations, expressions for a photodeflection normal signal are obtained. In every case this signal has the form

$$\begin{aligned} &F_n^{(p)} = K_n^{(p)} \mathrm{Re}[\vartheta_s(t) f_{ap}^{(p)}(z_D, z_l, z_p, h, h_D, \Omega, b_0, L)], \\ &(p) = (q), (c), \end{aligned} \tag{37}$$

where $K_n^{(p)}$ is the apparatus constant, $\vartheta_s(t) = \vartheta_g \exp[i(\Omega t + \gamma_g)]$ is the sample surface (complex) temperature, and $f_{ap}^{(p)}$ can be called the apparatus function (system sensitivity) of the experimental setup (also complex). In Appendix A expressions for $f_{ap}^{(c)}(h_D \to \infty)$ are given.

The knowledge of an apparatus function makes it possible to analyze the influence of various elements of the experimental setup on the measured signal. The influence of some parameters is well known, for example, screening the influence of the beam's height over sample h [20], as long as detector curtaining by the sample is not taken into account. This dependence has an exponential form resulting from the thermal wave dumping. The influence of other parameters is less examined in the literature, not counting earlier works where the complex geometric optics method was used (see, for example, [13]).

The results of simulation calculations of the dependence of apparatus complex function f_{ap} on various parameters of the experimental setup are shown below. Standard quantities taken for the calculations were as follows: $z_l = 0.5\,\mathrm{m}$, $z_p = 0.505\,\mathrm{m}$, $L = 0.5\,\mathrm{m}$, $z_D = 1.5\,\mathrm{m}$, $b_0 = 50\,\mu\mathrm{m}$, $f = 100\,\mathrm{Hz}$ (modulation frequency). If any of these values was a parameter in the calculations, then its changes were taken in the following sequences: $b_0 - 50, 100, 200, 400, 800, \ldots\,\mu\mathrm{m}$; $f - 100, 200, 400, 800, 1600, \ldots\,\mathrm{Hz}$; $z_l - 0.0, 0.25, 0.50, 0.75, 1.00, 1.25\,\mathrm{m}$. Moreover it was assumed at this point that in all calculations $I_{0D} = \mathrm{const}$.

An apparatus function dependence on the sample position z_l relative to the probing beam waist L and to the detector positions z_D is very interesting. This dependence is shown in Fig. 2, in the left column for the quadrant photodiode and in the right for the centroid one (in both cases without screening it was assumed that the probing beam axis height over the sample surface $h = 2b_s$, where b_s is the probing beam radius over the sample). It can be observed that the signal quickly vanishes when the sample is placed far from the probing beam waist (before or after this waist). This is due to the fact that when the sample is moved away from that waist the probing beam radius b_s is increased and the probing beam height over the sample needs to be increased too, for the reason that the sample cannot screen the probing beam. Next, because of large attenuation of a thermal wave with increasing h, the signal quickly vanishes. Moreover, from these graphs results, for narrow probing beams and for low frequency thermal field modulations it is extremely unfavorable when the sample is placed in the region of the probing beam waist, because in that case the apparatus function amplitude reaches its local minimum. Occurrence of these minima results from the fact that in the considered configuration the deflection part of a signal becomes insignificant. Most rays in the probing beam in the waist region run nearly parallel to one another and to the sample surface. Because the probing beam is narrow in comparison to the thermal wave length, rays undergo comparable deflection (in the beam waist area the refractive index gradient is almost constant) and it does not influence the probing beam divergence significantly. This minimum is quite narrow, which causes the apparatus function amplitude to be a quick-changing function in this region. This means that all instabilities of the relative position of the sample and the probing beam waist can significantly influence the measurement accuracy. It should be noted that the practice of locating the probing beam waist over the sample is quite common especially when a simple theory [1] is used to analyze photodeflection signals.

From the plots presented in Fig. 2, one can see the result that in the discussed ranges of the probing beam radii and thermal field modulation frequencies the apparatus function amplitude for both detectors reaches its maxima for the sample positions before as well as after the probing beam waist location. However, the favorable sample positions are before the probing beam waist for the quadrant diode and after this waist for the centroidal one. Of course this is only a qualitative suggestion but physically justified. From the comparison of formulas (34) and (36) it follows that normal signals are different in weighting function, which arises with amplitudinal correction a_{D1}; for the quadrant diode it is $\mathrm{sgn}(x_D) I_{G0x}(x_D)$ and for the centroid diode it is $x_D I_{G0x}(x_D)$. This means that in the case of the centroid diode greater importance is attached to rays deflecting from the probing beam axis, and there are more such rays if the sample is in the probing beam divergence area that is behind its waist. In the case of the quadrant diode the situation is the opposite—relatively greater importance is attached to the rays running close to the probing beam axis. And there are more such rays when the sample is in the probing beam convergence area that is before its waist. These differences result in such choice of the sample optimal position in relation to probing beam waist.

From Fig. 2 it can be additionally noted that the apparatus function amplitude depends also on the probing beam radius b_0. More detailed analysis about this dependency was carried out in Figs. 3 and 4. Similarly to what occurred previously, it was assumed that the sample does not screen the probing beam ($h = 2b_s$). It is visible that for both detectors these dependencies are very similar—some differences appear only for relative narrow probing beams ($b_0 < \mu_g$, where $\mu_g = 2\pi/k_g$ is the thermal wave length). In the investigated parameter value range, all the presented curves reach their maximal values, which corresponds to optimal values b_{opt} of the probing beam radii. Optimal probing beam radii obtained in this manner are presented in Fig. 4. As it is seen these values do not depend importantly on probing beam waist position L (see the upper row of Fig. 4) and generally for a centroid diode are greater than for quadrant one and depend on sample position z_l (see the bottom row of Fig. 4). It should be emphasized that the obtained optimal beam radii b_{opt} are relatively big—they are inside the range from nearly 200 to 700 μm. This is much greater than is used in standard experiments (e.g., [14,19]).

The normal photodeflection signal dependence on probing beam height h over the sample surface is very well known. In Figs. 2 and 3 this dependence is

manifested as an exponential decrease of the apparatus function amplitude with increasing probing beam diameter over the sample ($h = 2b_s$). Taking into account that the Gaussian beam after interaction with the thermal wave in the Raman–Nath configuration still remains Gaussian, it is possible to express probing beam cutting by a sample on the detector plane by the formulas

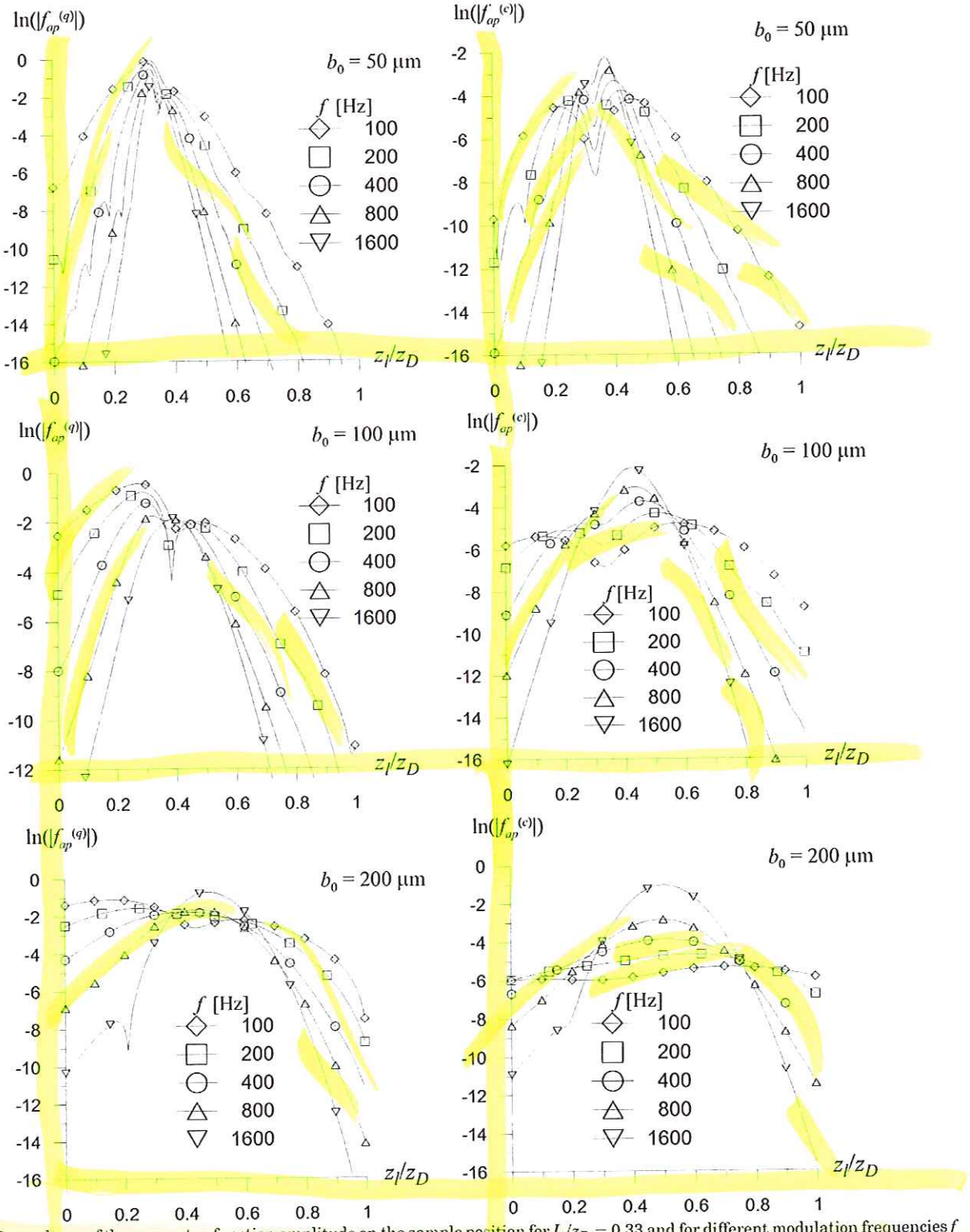

Fig. 2. Dependence of the apparatus function amplitude on the sample position for $L/z_D = 0.33$ and for different modulation frequencies f and for different probing beam radii b_0. Left column, quadrant diode; right column, centroid diode ($z_D = 1.5$ m, $\Delta z = 5$ mm).

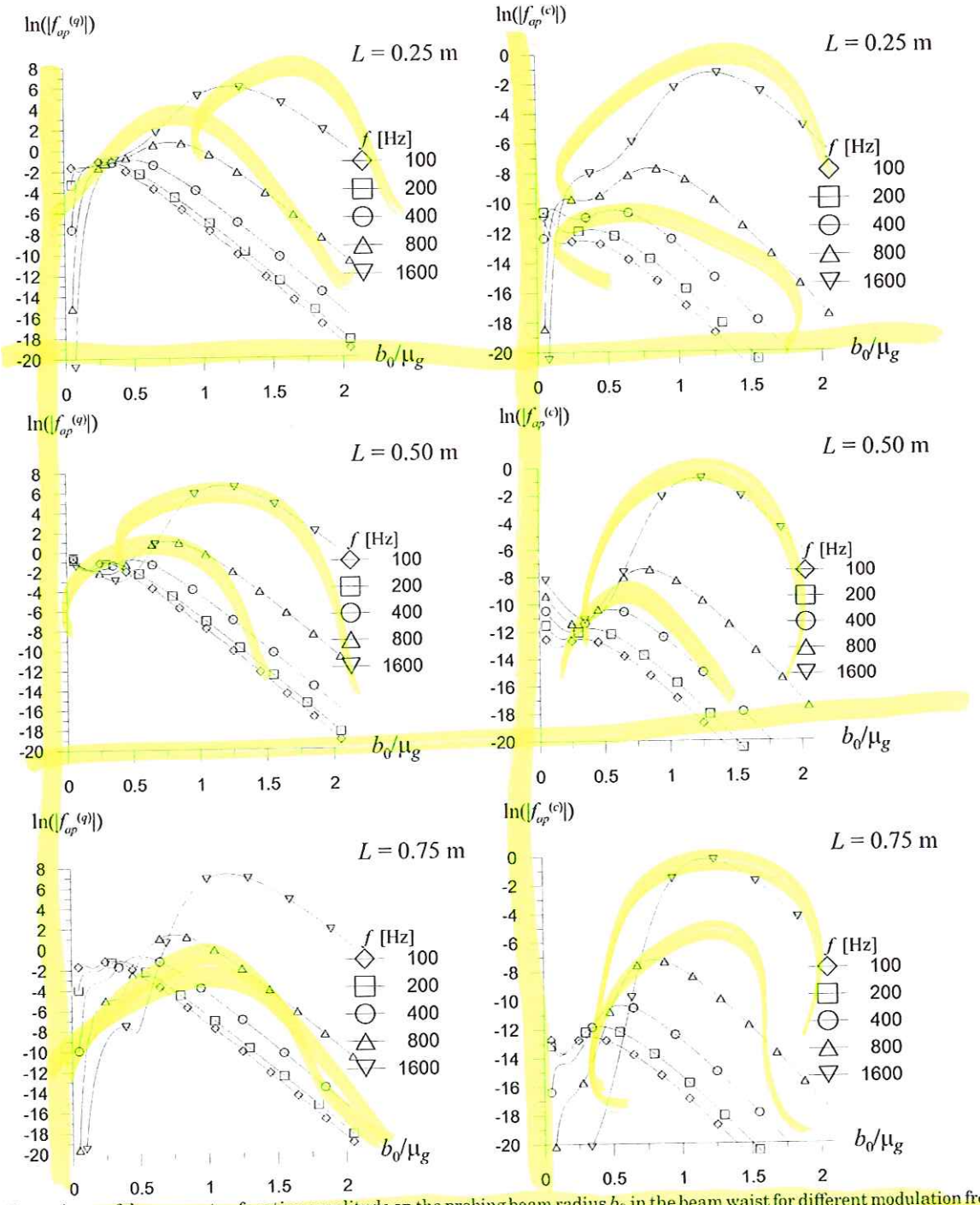

Fig. 3. Dependence of the apparatus function amplitude on the probing beam radius b_0 in the beam waist for different modulation frequencies f and for different probing beam waist positions L. Left column, quadrant diode; right column, centroid diode ($z_D = 1.5$ m, $\Delta z = 5$ mm).

$$h_D = h\sqrt{\frac{z_R^2 - (z_D - L)^2}{z_R^2 - (z_s - L)^2}}, \qquad z_s = \frac{z_l + z_p}{2}. \tag{38}$$

Here, the sample middle position is denoted by z_s. Of course, in this formulation any diffraction effects on the sample edges are omitted. Results of calculations are presented in Fig. 5. In all cases the minimal height of the probing beam axis over the sample surface was assumed as $h_{\min} = 0.05b_0$ (here $b_0 \cong b_s$, because it was simultaneously assumed that $z_l = L$, which means that in nearly all the experiments this assumption is fulfilled). As it is seen, when the probing beam height h over the sample surface increases the apparatus function amplitude first decreases, reaches its local minimum, next increases and reaches its maximal value, and finally decreases exponentially. It can be assumed that this maximal value of the apparatus

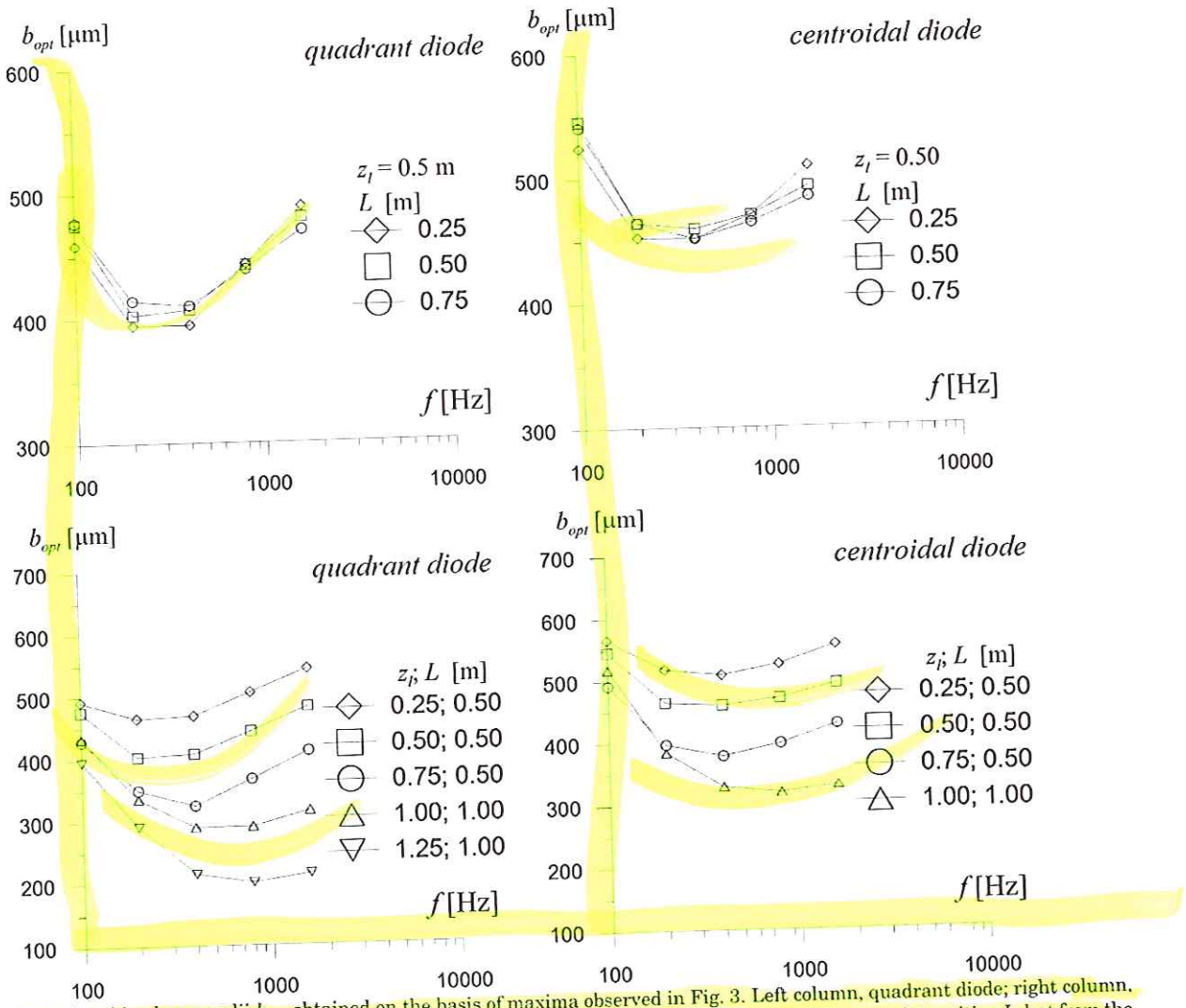

Fig. 4. Optimal probing beam radii b_{opt} obtained on the basis of maxima observed in Fig. 3. Left column, quadrant diode; right column, centroid diode. From the upper row it appears that the b_{opt} values practically do not depend on probing beam waist position L, but from the bottom row it is clear that they depend on sample position z_l.

function is reached for the optimal value of the probing beam height over the sample. Values of h_{opt} obtained in this manner are presented in Fig. 6. Generally it can be ascertained that the obtained optimal heights of the probing beam over the sample surface are greater for the centroid diode than for the quadrant diode (analogously to the calculated probing beam optimal radii). Moreover, in most cases the obtained h_{opt} values for given probing beams are greater then their radii b_0—for narrow beams ($b_0 < 100\,\mu$m) and for low modulation frequencies nearly two times. This means that in this situation the probing beam screening by sample is rather unimportant. However, in Fig. 5 it is seen that for these parameters and for very low heights of the probing beam over the sample the apparatus function amplitude reaches values greater then its maximal value in the last maximum. But this region is rather unprofitable because of the apparatus function's quick changeability, which can influence measurement accuracy. From Fig. 6 it is also seen that probing beam screening is not important for large probing beams interacting with thermal fields modulated at higher frequencies. In other cases the obtained h_{opt} values lie in probing beam screening regions.

5. Summary

We have analyzed an optical Gaussian beam interaction with a one-dimensional thermal wave in Raman–Nath configuration, in which we deal with a so-called normal photodeflection signal. For the description of that interaction the complex geometric optics methods and perturbation calculus was used. The phase, deflection, refractive, and amplitude corrections to the Gaussian optical beam rays were calculated. It was shown that for Gaussian beam eikonal all corrections mutually compensate, which means that probing beam after interaction with the thermal wave still stays Gaussian, but its intensity distribution is changed. The probing beam intensity distribution and "position" measurement was

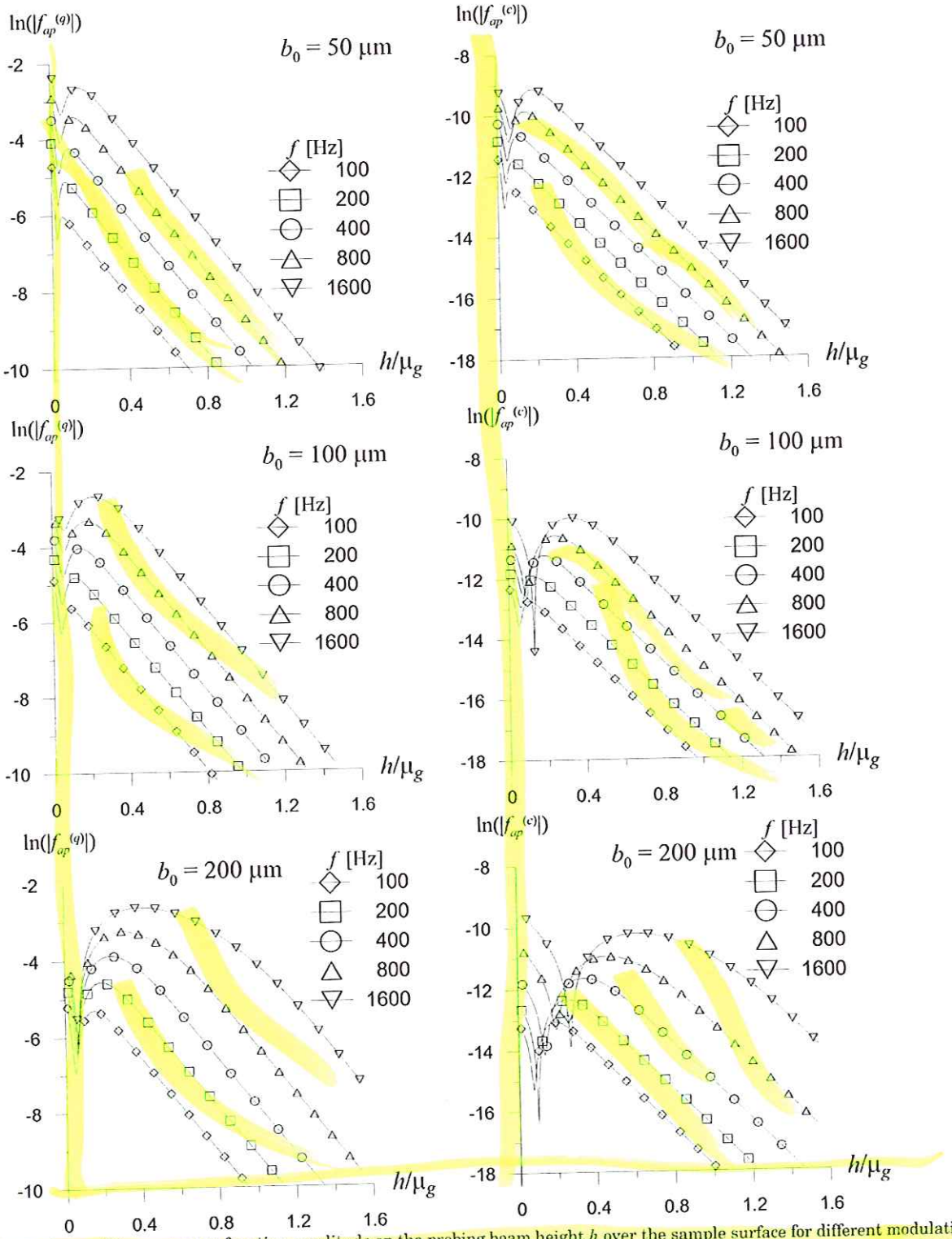

Fig. 5. Dependence of the apparatus function amplitude on the probing beam height h over the sample surface for different modulation frequencies f and for different probing beam radii b_0 in the beam waist. Left column, quadrant diode; right column, centroid diode ($z_D = 1.5$ m, $\Delta z = 5$ mm, $L = 0.5$ m, $z_l = 0.5$ m).

analyzed for two types of detector, a quadrant photodiode and a centroid one. Apparatus functions for the measurement setup for both detectors and for two cases, with and without probing beam screening, were obtained. The apparatus functions' dependencies on the sample position (for different probing beam waist locations), on the probing beam diameter, and on the probing beam height over the sample

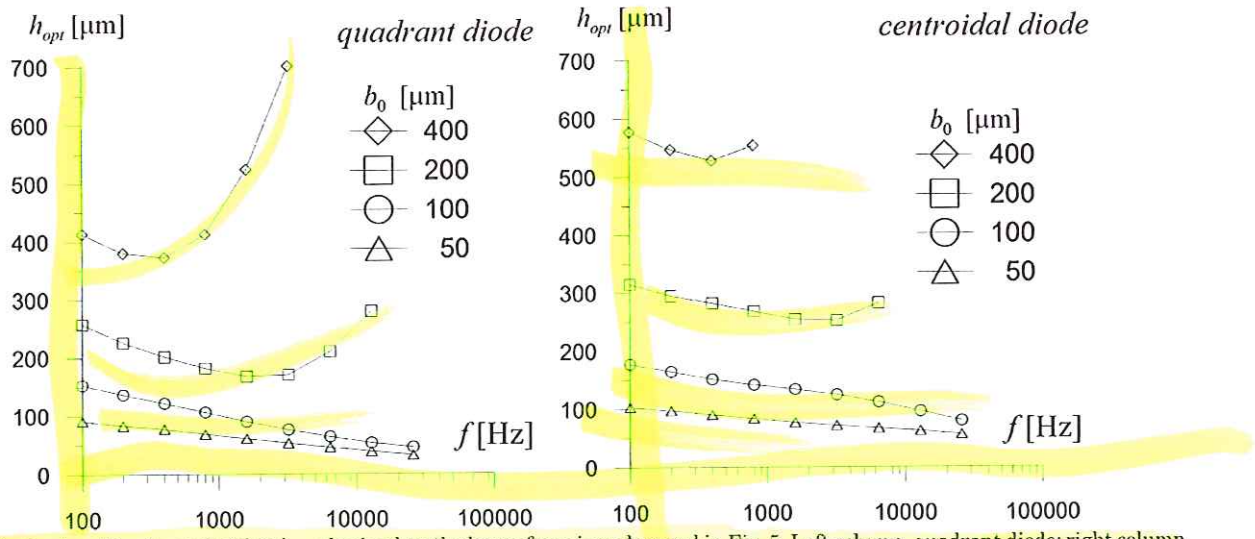

Fig. 6. Optimal probing beam heights h_{opt} obtained on the base of maxima observed in Fig. 5. Left column, quadrant diode; right column, centroidal diode.

were analyzed in detail. It was ascertained that the sample positioning in the probing beam waist region in most cases is unprofitable. It was proved that favorable sample positions are before the probing beam waist location for the quadrant diode and after this waist location for the centroid one (for the analyzed values of experimental setup parameters). The optimal values of the probing beam radii and the probing beam heights over the sample surface were determined as well. It was shown that most often the calculated probing beam optimal radii are greater than that traditionally used in experiments and that often the probing beam heights lay in the region of probing beam curtaining by the sample.

Appendix A

The expression for the apparatus function defined in Eq. (37) for the experimental setup presented in Fig. 1 with the centroid diode as the detector and without screening of the probing beam is

$$f_{ap}^{(c)} = \pi \exp(-k_{gc}h)\left[\frac{f_l}{4k_{gc}z_{RD}^3}\exp\left(\frac{b_D^2k_{gc}^2}{4z_{RD}^2}z_{Rl}^2\right) - \frac{f_p}{4k_{gc}z_{RD}^3}\exp\left(\frac{b_D^2k_{gc}^2}{4z_{RD}^2}z_{Rp}^2\right) + f_{pl}\right], \tag{A1}$$

where

$$f_r = b_D^4k_{gc}^2z_{Rr}(z_{RD}^2 - 2z_{RD}z_{Rc} + 2z_{Rc}z_{Rr}) + 2b_D^2z_{RD}^2[k_{gc}^2z_{RD}z_{Rr}(z_{RD} - z_{Rr}) + 2(z_{RD} - z_{Rc}) + 8z_{RD}^5]; \quad r = l,p, \tag{A2}$$

$$f_{pl} = i\sqrt{\pi}b_Dz_{RD}^2\left[\exp\left(\frac{ib_Dk_{gc}}{2z_{RD}}z_{Rl}\right) - \exp\left(\frac{ib_Dk_{gc}}{2z_{RD}}z_{Rp}\right)\right], \tag{A3}$$

$$k_{gc} = (1+i)k_g, \qquad b_D = b_0\sqrt{1 + \frac{(z_D - L)^2}{z_R^2}}, \tag{A4}$$

$$z_{Rr} = z_{Rc} + iz_r, \qquad r = l,p,D, \tag{A5}$$

$$z_{Rc} = z_R - \mathrm{iL}, \qquad z_R = k_0n_0b_0^2, \qquad k_g = \sqrt{\Omega/(2\kappa_g)}. \tag{A6}$$

References

1. C. Murphy and L. C. Aamodt, "Photothermal spectroscopy using optical beam probing: mirage effect," J. Appl. Phys. **51**, 4580–4588 (1980).
2. L. C. Aamodt and C. Murphy, "Photothermal measurement using localised excitation source," J. Appl. Phys. **52**, 4903–4914 (1981).
3. F. A. McDonald and G. C. Wetsel, Jr., "Resolution and definition in thermal imaging," *Proceedings of the 1984 Ultrasonics Symposium* (IEEE, 1984), pp. 622–628.
4. F. A. McDonald, G. C. Wetsel, Jr., and G. E. Jamieson, "Photothermal beam-deflection imaging of vertical interfaces of solids," Can. J. Phys. **64**, 1265–1268 (1986).
5. E. L. Lasalle, F. Lepoutre, and J. P. Roger, "Probe beam size effects in photothermal deflection experiments," J. Appl. Phys. **64**, 1–5 (1988).
6. H. S. Carslaw and J. C. Jaeger, *Conduction of Heat in Solids* (Oxford U. Press, Oxford, 1959).
7. R. J. Bukowski, "Optical gaussian beam in acoustooptics. Theoretical description of noncollinear isotropic interactions," Proc. SPIE **5828**, 1–15 (2005).
8. A. Glazov and K. Muratikov, "Photodeflection signal formation in thermal wave spectroscopy and microscopy of solids within the framework of wave optics. "Mirage" effect geometry," Opt. Commun. **84**, 283–289 (1991).
9. A. Glazov and K. Muratikov, "Calculation of photodeflection signal in the framework of wave optics," Tech. Phys. **38**, 344–352 (1993).

10. R. J. Bukowski, "Mirage effect description in the frame of complex rays optics," Proc. SPIE **3581**, 285–292 (1998).
11. R. J. Bukowski and D. Korte, "Gaussian beam phase change and deflection in temperature field of thermal wave," presented at the Workshop 2001—Photoacoustics and Photothermics, Ebernburg, Germany, 26–28 September 2001.
12. D. Kobylinska, R. J. Bukowski, B. Burak, J. Bodzenta, and S. Kochowski, "The complex ray theory of photodeflection signal formation—comparison with the ray theory and experimental results," J. Appl. Phys. **100**, 063501 (2006).
13. D. Kobylinska, R. J. Bukowski, B. Burak, J. Bodzenta, and S. Kochowski, "Photodeflection signal formation in photothermal measurements—comparison of the complex ray theory, the ray theory, the wave theory, and experimental results," Appl. Opt. **46**, 5216–5227 (2007).
14. D. K. Kobylińska, R. J. Bukowski, J. Bodzenta, S. Kochowski, and A. Kaźmierczak-Bałata, "Detector effects in photothermal deflection experiments," Appl. Opt. **47**, 1559–1566 (2008).
15. J. Petykiewicz, *Wave Optics* (Kluwer, 1992).
16. Yu. A. Kravcov and Yu. I. Orlov, *Geometrical Optics of Inhomogeneous Media* (WNT, 1993) [Polish edition].
17. Yu. A. Kravtsov, "Complex rays and complex caustics," Radiophys. Quantum Electron. **10**, 719–730 (1967).
18. J. B. Keller and W. Streifer, "Complex rays with applications to Gaussian beams," J. Opt. Soc. Am. **61**, 40–43 (1971).
19. J. C. Power and M. A. Schweitzer, "Diffraction theory of the impulse mirage effect," Opt. Eng. **36**, 521–534 (1997).
20. J. Bodzenta, "Thermal wave method in investigation of thermal properties of solids," Eur. Phys. J. Spec. Top. **154**, 305–311 (2008).